ORIGINAL PAPER

A multiresolution approach for enhancement and denoising of microscopy images

Ufuk Bal · Mehmet Engin · Urs Utzinger

Abstract In order to overcome blurring due to microscope optics in fluorescence microscopy, we propose a wavelet transform-based non-iterative blind deconvolution method. In our proposed deconvolution algorithm, we used wavelet-based denoising algorithms. We compared discrete wavelet transform (DWT) and wavelet packet transform (WPT) structures as denoising algorithms. WPT-based algorithm resulted in less error than the DWT-based algorithm. Minimum error was obtained for coif5 wavelet type. We compared our denoising methods with several standard denoising methods. Also, we compared our proposed deconvolution algorithm with several standard deconvolution methods. Our proposed wavelet transform-based deconvolution method resulted in the least error compared to other methods. To test the efficacy of our deconvolution method on cell images, we proposed a wavelet entropy-based non-reference image quality (contrast enhancement) metric. We tested our proposed metric by increasing blurring ratio both for noiseless and noisy images. Our metric is useful for evaluating image quality in terms of deblurring.

U. Bal (✉)
Information Systems Engineering, Mugla University,
48000 Mugla, Turkey
e-mail: ufukbal@mu.edu.tr

M. Engin
Electrical and Electronics Engineering Department,
Ege University, 35100 Izmir, Turkey

U. Utzinger
Biomedical Engineering, 1127 E James E. Rogers Way,
Tucson, AZ 85721, USA

1 Introduction

Image quality obtained in fluorescence microscopy is limited by blurring due to microscope optics which can be modeled as point spread function (PSF) and noise due to the photo-detection process. Photon counting noise which results from the probabilistic nature of photon emission is the major source of noise in fluorescence imaging [1]. This inherent randomness in the emission rate of photons is well described by a Poisson process [2]. In addition to photon counting noise, noise contributions, such as electronic thermal noise, readout noise, background noise, also exist. When all put together, these noise contributions can be considered as normally distributed [2]. However, since live samples are often observed at very low light levels, detector noise is often limited to only photon counting noise [1].

Deconvolution and denoising can be used to restore the images that were degraded by blurring and noise. On blurring of microscopic images, researchers have applied several algorithms: Linear, nonlinear, blind, non-blind, iterative, non-iterative and statistical algorithms exist in the literature. Due to large datasets in microscopy imaging, deconvolution algorithms requiring less processing time are preferable.

Linear methods such as Inverse Filtering and Wiener Filtering are the simplest deconvolution methods. They are useful for moderate noise levels. Implementation efficiency in the Fourier domain is one of the advantages of linear methods. Nevertheless, these methods are very sensitive to errors in the PSF data used for the estimation of deconvolved images [3].

In order to overcome the difficulties that present in linear methods, nonlinear methods have been exploited; however, they require incorporating constraints such as non-negativity. Due to these constraints, computational complexity of nonlinear iterative algorithms increases. And these methods have

limited noise reduction capabilities compared to statistical methods.

Statistical methods such as maximum likelihood and Bayesian methods are effective in the presence of high noise levels. But they have larger computational requirements than linear and nonlinear methods [4].

All algorithms mentioned above assume that the PSF is known, which is difficult in practice. An experimentally measured PSF always exhibits some noise. Theoretically calculated PSF cannot foresee all microscopy-related parameters. Blind deconvolution algorithms simultaneously estimate the PSF and a sharp image from the degraded image. In the literature, the most discussed iterative blind deconvolution algorithm is the Richardson–Lucy (RL) algorithm [5–7]. Several researchers used the maximum a posteriori (MAP) estimation approach to blind deconvolution [8,9]. Levin et al. derived a simple approximated MAP algorithm [8] which uses a different kernel update system from common MAP approaches. Since these methods are iterative, additional processing time is required compared to non-iterative methods.

SeDDaRA (self-deconvolving data reconstruction algorithm) [10,11] is a Fourier-based, non-iterative, blind deconvolution algorithm. The method does not require knowledge of the point spread function. It is based on finding a suitable representation of the scene [11]. Since SeDDaRA is non-iterative, it can be implemented quickly while effectively deblurring the image [11]. Also, SeDDaRA can be performed without prior knowledge of the detection system. Due to its advantages over Fourier transform, the wavelet transform became popular for denoising [12–14], image compression [15–17], edge detection [18] and deconvolution [12,19,20] applications. In this study, in order to combine the advantages of SeDDaRA and wavelet transform, the SeDDaRA algorithm was modified using wavelets.

Algorithms for deconvolution of microscopic images can be two dimensional or three dimensional. Two-dimensional methods apply an operation to each plane of a three-dimensional image stack separately. In contrast, three-dimensional methods operate simultaneously on every voxel in a three-dimensional image stack. While our proposed deconvolution method uses a two-dimensional approach, other methods mentioned above can use either two- or three-dimensional approach. Two-dimensional methods are computationally economical because they involve relatively simple calculations performed on single image planes. For example, in confocal imaging, a single confocal image can be rapidly deconvoluted with 2D deconvolution by applying a 2D PSF [21,22]. Such an approach improves the image quality because the depth of field of a confocal microscope is thin [23]. However, some 2D methods, such as neighboring methods, have several disadvan-

tages. For one, they are not efficient at removing the noise, since noise from several planes tends to get added together [24].

In order to overcome noise, our modified SeDDaRA algorithm includes a wavelet-based denoising process. In general, denoising methods based on the wavelet transform consist of three steps: (1) calculate the wavelet transform of the noisy image (decomposition), (2) modify the wavelet coefficients according to some rule (thresholding) and (3) calculate the inverse transform using the modified wavelet coefficients (reconstruction). The main assumption of this type of denoising (thresholding) is that the small coefficients are dominated by noise, while coefficients with a large absolute value carry more signal information. Thresholding of the coefficients might be global or level dependent, hard or soft, based on a priori known or estimated noise statistics [25].

There are several wavelet-based denoising methods applicable for fluorescence microscopy when noise is described by a Poisson process. One approach, called Pure-let, is based on the minimization of an unbiased estimate of the mean square error (MSE) for Poisson noise and the preservation of Poisson statistics across scales within the Haar discrete wavelet transform (DWT) [26]. Using a similar approach, we determined threshold values for wavelet coefficients based on approximation coefficients at the same scale.
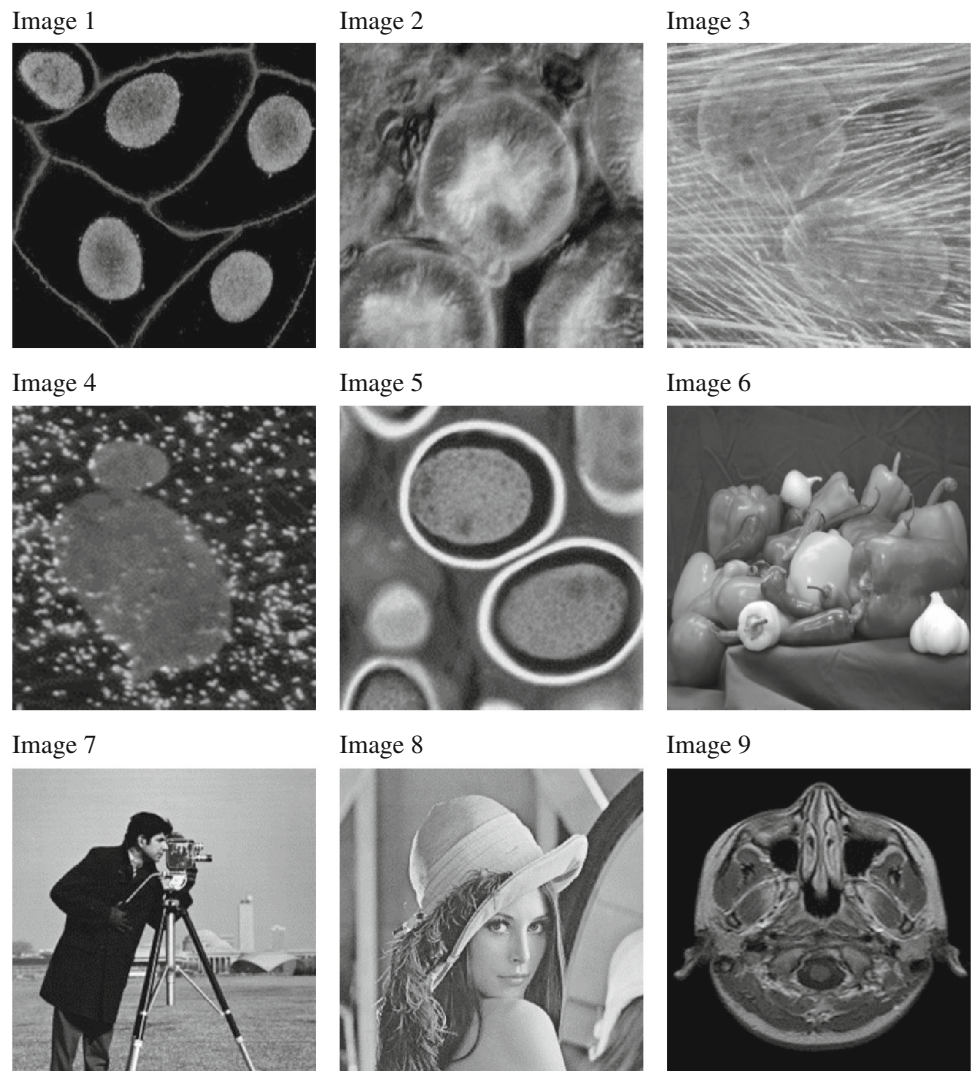
Mean square error (MSE) and peak signal to noise ratio (PSNR) are image quality metrics which can be used only when a noise-free reference image is known. But in practice, it is often not possible to know such a reference image. Therefore, we developed a wavelet entropy-based non-reference image quality metric and also measured the performance of our algorithm.

2 Materials and methods

The cells expressing fluorescent proteins and the test images are used to evaluate the performance of the proposed deconvolution model and image quality metrics.

2.1 Test images

In order to validate our methods, we used nine test images (Fig. 1). Five of them are microscopic images that were taken from Nikon and Olympus Fluorescence Microscopy Digital Image Gallery websites (Madin-Darby Canine Kidney Epithelial Cells, Mouse Kidney Tissue, African Water Mongoose Skin Fibroblast Cells, Tahr Ovary Epithelial Cells, Human Roundworm). Three of them are standard test images (Peppers, Cameraman, Lena), and the last one is an MRI.

Fig. 1 Test images

Image 1

Image 2

Image 3

Image 4

Image 5

Image 6

Image 7

Image 8

Image 9

2.2 Cells

Imaging of DsRed2 (Discosoma sp. Red Fluorescent Protein variant 2) and eGFP (enhanced Green Fluorescent Protein) labeled cells (MCF-7 breast cancer cells) was performed with a single beam intravital microscope (TrimScope, LaVision BioTec, Bielefeld, Germany, objective lens: $20 \times$ NA:0.95, XLUMPLFL, Olympus) and a Zeiss Laser Scanning Microscope (LSM 510, Carl Zeiss Microscopy, Jena, Germany, objective lens: $40 \times$ NA:1.0 W.I. W Plan-Apochromat). Cytosol was labeled with DsRed2 and the nucleus with eGFP. Images were recorded over 40μm deep with a step size of 1μm.

2.3 Two-dimensional DWT

In classical signal processing, it is typical to assume the low-pass content is signal and the high-pass content is noise. Hence, the conventional fast Fourier transform (FFT)-based image denoising is essentially based on applying a low-pass filter to the noisy image. Unfortunately, many signals of interest have important high-pass features, and simple low-pass filtering diminishes or removes these features. The attenuation of the high-frequency components would result in an undesirable blurring of the edges [27,28]. Unlike Fourier transform, wavelet transform shows localization in both time and frequency. The localized nature of the wavelet transforms both in time and frequency results in denoising with edge preservation [29,30].

The discrete wavelet transform of function $f(x, y)$ of size $M \times N$ is

$$W_{\varphi}(j_0, m, n) = \frac{1}{\sqrt{MN}} \sum_{0}^{m-1} \sum_{0}^{n-1} f(x, y) \varphi_{j0,m,n}(x, y)$$

$$W_{\psi}^{i}(j, m, n) = \frac{1}{\sqrt{MN}} \sum_{0}^{m-1} \sum_{0}^{n-1} f(x, y) \psi_{j,m,n}(x, y) \quad (1)$$

$$i = \{H, V, D\}$$

where W_φ and W_ψ represent the approximation and detail (wavelet) coefficients, φ and ψ are the basis functions, index i identifies the horizontal, vertical and diagonal details, j represents the scale, j_0 is an arbitrary starting scale, and m, n are the position-related parameters [31].

Denoised image is obtained by performing inverse DWT after modifying the wavelet coefficients according to some rules. Given the W_φ and W_ψ of Eq. 1, $f(x, y)$ is obtained via the inverse discrete wavelet transform

$$f(x, y) = \frac{1}{\sqrt{MN}} \sum_m \sum_n W_\varphi(j_0, m, n)\varphi_{j_0,m,n}(x, y)$$
$$+ \frac{1}{\sqrt{MN}} \sum_{i=H,V,D} \sum_{j=j_0}^{\infty} \sum_m \sum_n W_\psi^i(j, m, n)\psi_{j,m,n}^i(x, y) \quad (2)$$

Wavelet packet transform (WPT) is a generalization of DWT. While in DWT, only the approximations at each resolution level are decomposed to yield approximation and detail information at a higher level, in the wavelet packet analysis, both the approximation and details are decomposed [32].

2.4 Denoising method used in modified SeDDaRa

Our proposed deconvolotion algorithm incorporates denoising.

A two-level wavelet transform was performed on degraded data. Detail coefficients were filtered using an e-median (epsilon median) filter (3×3 window size based) for each level. E-median filter can be defined as:

$$f(x, y) = g_m(x, y) + X(g(x, y) - g_m(x, y))$$
$$X(x) = \begin{cases} x, & |x| > \lambda \\ 0 & \text{otherwise} \end{cases} \quad (3)$$

where $g(x, y)$ represents the degraded data, $g_m(x, y)$ represents the median filtered data, and λ represents the threshold value [33]. The e-median filter preserves edges while removing noise [33,34]. In Poisson processes, the noise is stationary and completely described by its variance. Also, approximation coefficients and detail coefficients are statistically correlated [26,35]. Thus, we used square root of the approximation coefficients as threshold values. This quantity can be considered as an estimate of the local standard deviation [26].

$$T_j = \text{constant} \times \sqrt{a_{j1}^2 + a_{j2}^2 + \cdots a_{jn}^2}$$
$$\text{constant} \sim \frac{1}{\sqrt{mn}} \quad (4)$$

where j, a_j and mn represent the level of wavelet transform, approximation coefficients and image size, respectively.

For Gaussian noise processes, our method uses the same threshold values as for Poisson processes (formula 4).

When examining algorithms based on DWT, the mother wavelet type was chosen by comparing the effect of different mother wavelet types on our denoised images. The optimal type was the mother wavelet that minimizes the error between reference and denoised image.

Algorithms based on WPT used the same procedures as the DWT algorithm; however, the required coefficients were generated by two-level wavelet packet decomposition.

After thresholding of coefficients, images were reconstructed with inverse discrete wavelet transform.

We compared our proposed denoising method with several standard denoising approaches: DWT- and WPT-based soft and hard thresholding denoising [36–38] and Pure-let denoising [26].

2.5 Modified SeDDaRA

SeDDaRA is a Fourier-based, non-iterative, blind deconvolution algorithm. Derivation of SeDDaRA can be summarized as follows:

Generally, in any imaging system, degraded data $g(x, y)$ can be modeled as;

$$g(x, y) = f(x, y) \times d(x, y) + w(x, y) \quad (5)$$

where $f(x, y)$ represents the ideal reference image, $d(x, y)$ represents the PSF, and $w(x, y)$ denotes the noise component, respectively. Objective is to find the best estimate of $f(x, y)$ from the degraded data $g(x, y)$ when PSF and noise are unknown. Taking the Fourier transform of Eq. 5;

$$G(u, v) = F(u, v)D(u, v) + W(u, v) \quad (6)$$

The deconvolution with a pseudoinverse filter is given by

$$F(u, v) = \frac{G(u, v)D^*(u, v)}{|D(u, v)|^2 + K} \quad (7)$$

where D^* is the complex conjugate of D. The constant K acts as a tuning parameter to guard against amplification of the image noise. For SeDDaRA [10], $D(u, v)$ is given by

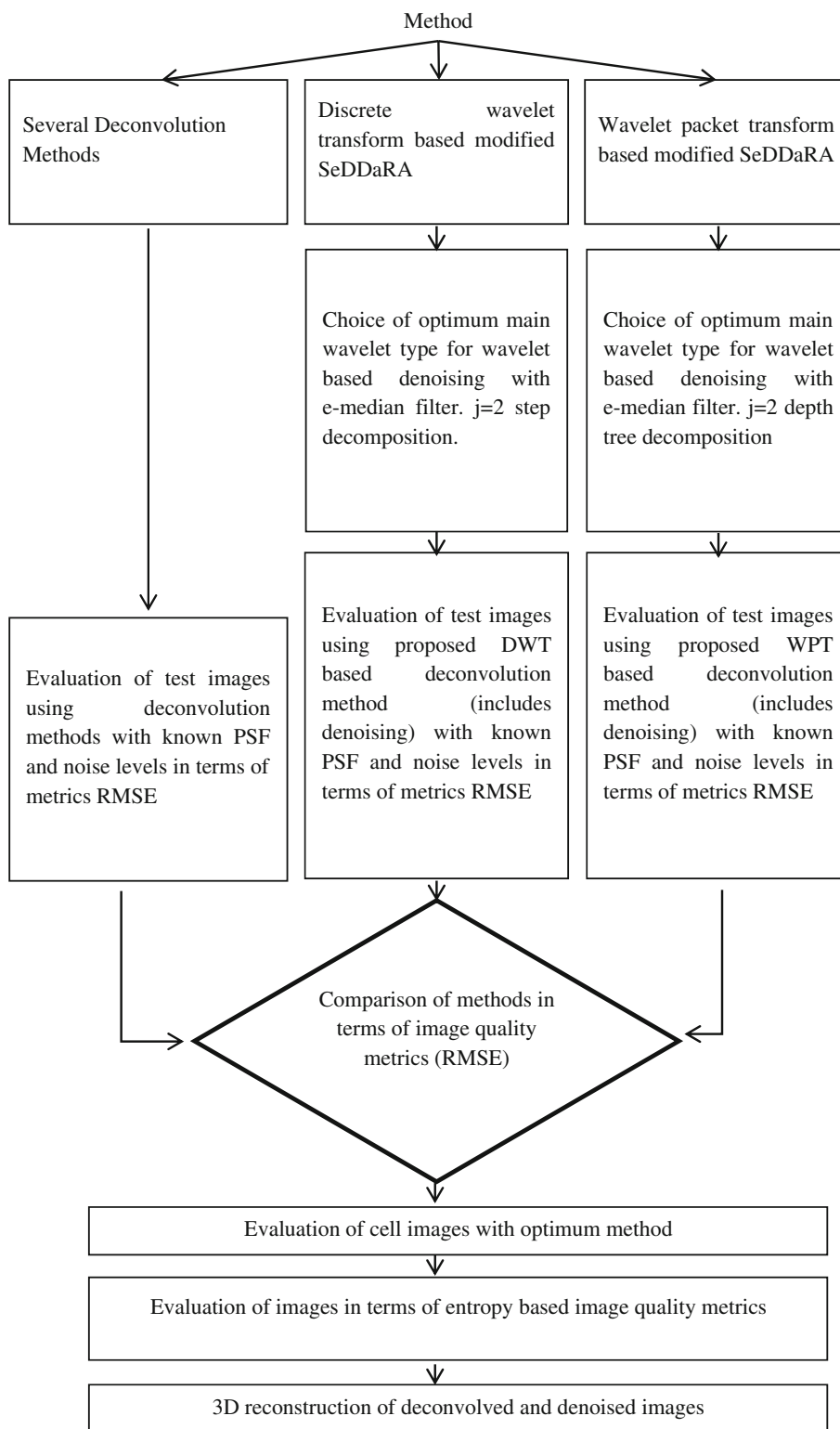$$D(u, v) = [K_G S\{|G(u, v) - W(u, v)|\}]^{\alpha(u,v)} \quad (8)$$

where $\alpha(u, v)$ is a tuning parameter and K_G is a real, positive scalar chosen to ensure $|D(u, v)| \leq 1$. $S\{\ldots\}$ [35] means application of smoothing filter. $\alpha(u, v)$ must be chosen as $0 \leq \alpha(u, v) < 1$. $D(u, v)$ is the Fourier transform of the PSF.

By assuming $W(u, v)$ is negligible Carron obtained $D(u, v)$ as:

$$D(u, v) = [K_G S\{|G(u, v)|\}]^{\alpha(u,v)} \quad (9)$$

where $K_G = 1/Max[S\{|G(u, v)|\}]$.

Fig. 2 Flow diagram of image enhancement

Our proposed SeDDaRA uses wavelet transform instead of a Fourier transform when applying a smoothing filter to degraded data

$$g_d(x, y) = S_w\{g(x, y)\} \tag{10}$$

where $g_d(x, y)$ represents the denoised data and $S_w\{\ldots\}$ means smoothing in wavelet domain. For obtaining an estimation of the PSF and for denoising purposes, we used smoothed data in Eqs. 7 and 9. If we rewrite Eqs. 7 and 9, we obtain as follows:

Table 1 Comparison of different mother wavelet types in our DWT-based denoising method for poisson corrupted image

Wavelet type	Noisy image RMSE	Denoised image RMSE
Haar	5.287 ± 0.026	5.299 ± 0.026
db2	5.288 ± 0.025	5.195 ± 0.023
db4	5.289 ± 0.025	5.195 ± 0.026
coif5	5.290 ± 0.025	5.100 ± 0.027
sym2	5.288 ± 0.023	5.195 ± 0.025
sym4	5.287 ± 0.026	5.122 ± 0.028
bior1.1	5.282 ± 0.023	5.299 ± 0.023
bior1.5	5.282 ± 0.027	5.432 ± 0.028
dmey	5.287 ± 0.024	5.47 ± 0.022

Table 2 Comparison of different mother wavelet types in our WPT-based denoising method for Poisson corrupted image

Wavelet type	Noisy image RMSE	Denoised image RMSE
Haar	5.286 ± 0.027	5.366 ± 0.027
db2	5.284 ± 0.024	5.201 ± 0.025
db4	5.287 ± 0.026	5.076 ± 0.026
coif5	5.285 ± 0.021	4.998 ± 0.023
sym2	5.285 ± 0.026	5.205 ± 0.026
sym4	5.286 ± 0.024	5.076 ± 0.026
bior1.1	5.289 ± 0.027	5.368 ± 0.029
bior1.5	5.287 ± 0.025	5.587 ± 0.025
dmey	5.288 ± 0.027	5.32 ± 0.022

$$D(u, v) = [K_G \Im \{g_d(x, y)\}]^{\alpha(u,v)}$$
$$F(u, v) = \frac{\Im \{g_d(x, y)\} D^*(u, v)}{|D(u, v)|^2 + K} \tag{11}$$

where $\Im$ is the Fourier transform operator. Thus, our proposed method combines denoising and the deconvolution processes. Estimation of $(D(u, v))$ was obtained by substituting the smooth image $\Im \{|g_d(x, y)|\}$ into Eq. 11 while $\alpha(u, v)$ was chosen as a constant number between (0,1).

Expressing the Eq. 9 as a power-law relation enables one to approximate $\alpha(u, v)$ as a constant [10]. Substituting $D(u, v)$ and $\Im \{|g_d(x, y)|\}$ into Eq. 11 and taking the inverse Fourier transform, we obtained an estimation of the ideal image. In Eq. 11, K was chosen as 1 % of the average of $|D(u, v)|$.

We used artificially blurred and noisy test images to compare our deconvolution method with several standard deconvolution methods in terms of RMSE.

2.6 Derivation of image quality metrics

Generally, image quality may be evaluated using MSE and PSNR when a reference image is available.

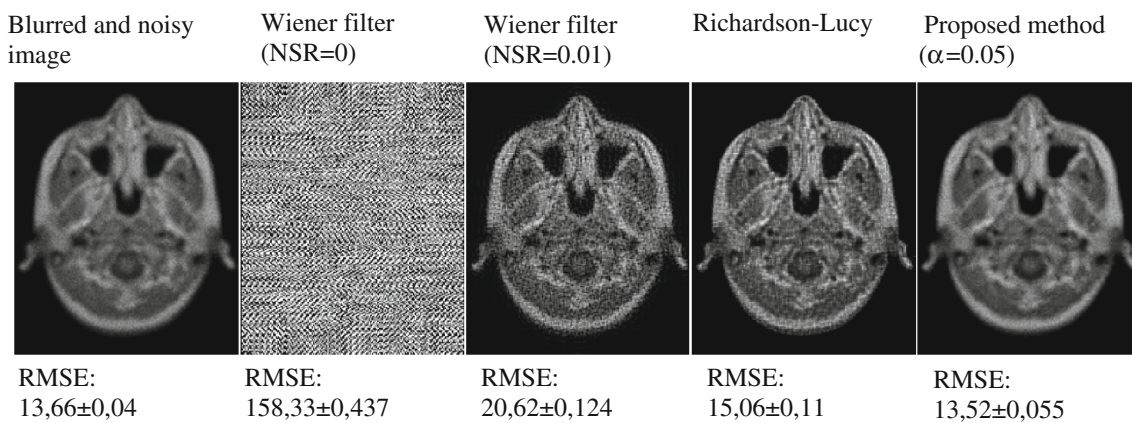$$MSE = \frac{1}{mn} \sum_{i=0}^{m-1} \sum_{j=0}^{n-1} [g(i, j) - f(i, j)]^2 \tag{12}$$

$$PSNR = 10 \log_{10} \frac{max_i^2}{MSE} = 20 \log_{10} \frac{max_i}{RMSE} \tag{13}$$

where max_i represents the maximum pixel value (255 for 8 bits e.g.) and root mean square error (RMSE) defined as the square root of the MSE. For a good quality image, the PSNR value should be high and the MSE value should be low. PSNR is a good measure for comparing restoration results for the same image, but between-image comparisons of PSNR are meaningless.
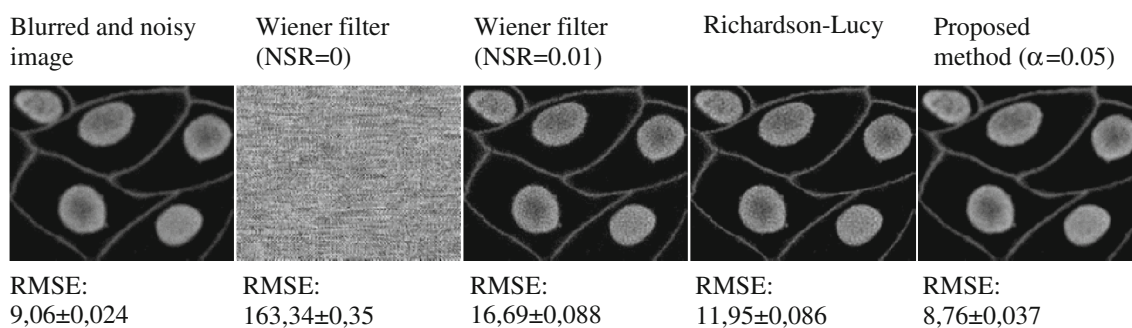
In order to evaluate image quality without a reference image, we need other quality metrics. One choice for non-reference image quality assessment is entropy-based methods. Entropy-based methods [39,40] were modified, and a quality assessment parameter was derived the following way: For each pixel in the image, we obtained subimages using a sliding window (size 9×9). The subimages were transformed to one-dimensional vectors. A two-level DWT ($L = 2$) was performed for each pixel vector. An entropy image was calculated with the wavelet entropy of pixel vectors. The wavelet entropy is given by as follows:

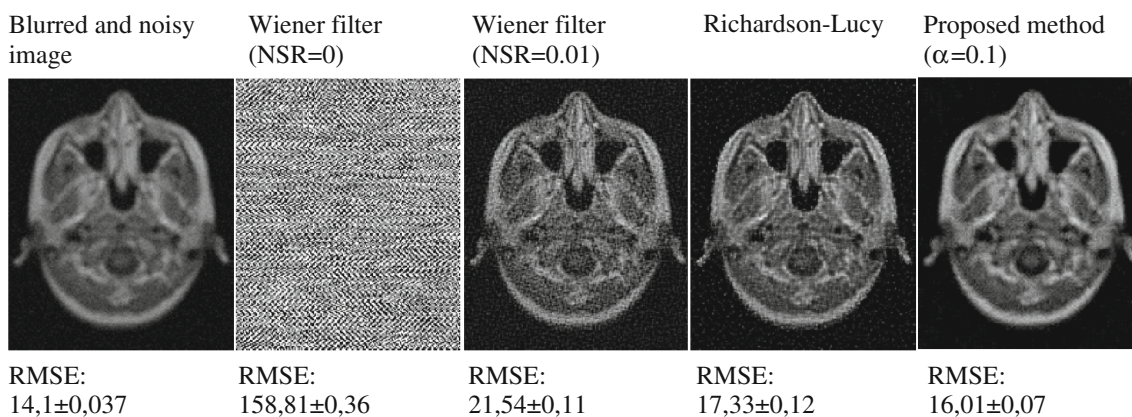**Table 3** Comparison of denoising methods for Poisson corrupted images

	Image 1	Image 2	Image 3	Image 4	Image 9
Noisy İmage	5.29 ± 0.025	9.58 ± 0.038	11.24 ± 0.038	7.62 ± 0.042	6.25 ± 0.034
DWT-hard thresholding	5.25 ± 0.025	7.39 ± 0.033	11.074 ± 0.042	11.44 ± 0.058	6.01 ± 0.062
WPT-hard thresholding	5.25 ± 0.025	9.58 ± 0.043	11.238 ± 0.037	7.61 ± 0.039	6.21 ± 0.035
DWT-soft thresholding	4.19 ± 0.020	7.88 ± 0.022	12.57 ± 0.025	14.37 ± 0.036	5.56 ± 0.24
WPT-soft thresholding	4.25 ± 0.021	9.58 ± 0.043	11.238 ± 0.037	7.61 ± 0.039	5.10 ± 0.035
Proposed DWT-based method	5.16 ± 0.026	7.70 ± 0.044	9.91 ± 0.045	7.47 ± 0.045	6.01 ± 0.037
Proposed WPT-based method	5.00 ± 0.024	7.57 ± 0.045	9.53 ± 0.041	7.23 ± 0.044	5.86 ± 0.039
Pure-Let	4.03 ± 0.019	6.40 ± 0.024	8.01 ± 0.027	6.52 ± 0.041	5.18 ± 0.028

Fig. 3 Comparison of proposed method with non-blind deconvolution methods for artificially blurred MRI corrupted by Poisson noise. Test image was blurred by convolving image with a 5×5 Gaussian filter
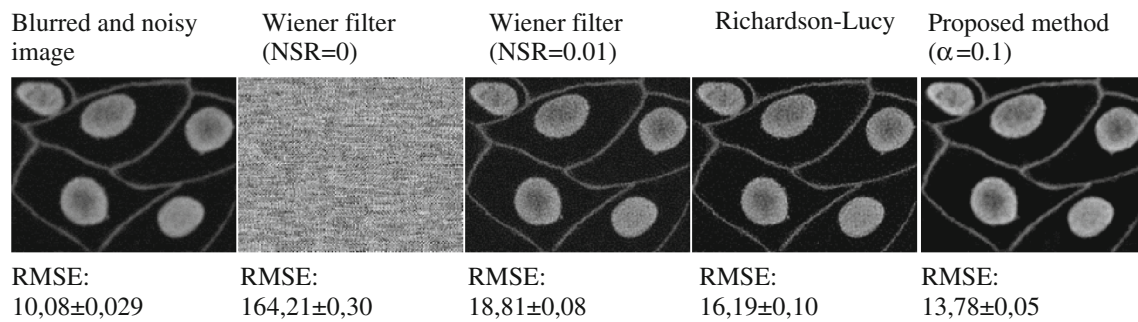

Fig. 4 Comparison of proposed method with non-blind deconvolution methods for artificially blurred microscopic image corrupted by Poisson noise. Test image was blurred by convolving image with a 5×5 Gaussian filter

Fig. 5 Comparison of proposed method with non-blind deconvolution methods for artificially blurred MRI corrupted by Gaussian noise. Test image was blurred by convolving image with a 5×5 Gaussian filter

$$e = -\sum_{j=1}^{L} pj \log_2 pj$$

$$pj = \frac{E_j}{E_t} = \frac{E_{dj}}{E_{aL} + \sum_{j=1}^{L} E_{dj}}$$

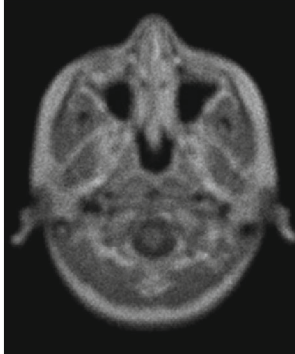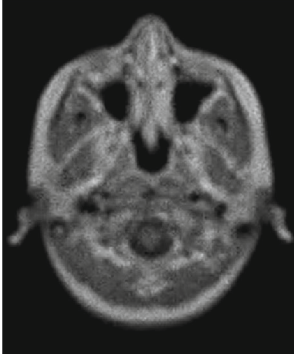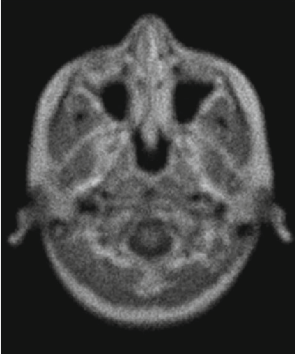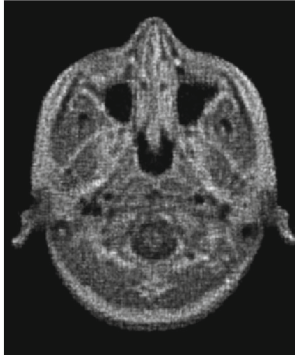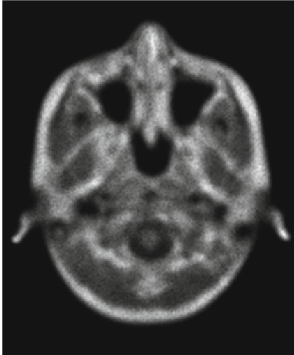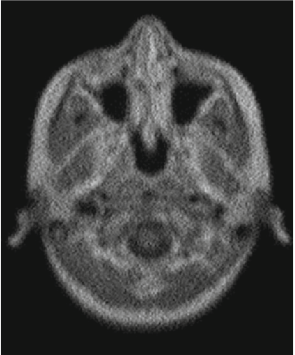$$E_{aj} = a_{j1}^2 + a_{j2}^2 + \cdots a_{jn}^2$$

$$E_{dj} = d_{j1}^2 + d_{j2}^2 + \cdots d_{jn}^2 \qquad (14)$$

where E_j, E_t, a_j and d_j represent the wavelet energy of j_{th} level, total energy of all levels, approximation coefficients and detail coefficients, respectively [41]. The wavelet energy is defined as total square of the wavelet coefficients for the corresponding level.

Blurred and noisy image	Wiener filter (NSR=0)	Wiener filter (NSR=0.01)	Richardson-Lucy	Proposed method (α=0.1)

RMSE: 10,08±0,029	RMSE: 164,21±0,30	RMSE: 18,81±0,08	RMSE: 16,19±0,10	RMSE: 13,78±0,05

Fig. 6 Comparison of proposed method with non-blind deconvolution methods for artificially blurred microscopic image corrupted by Gaussian noise. Test image was blurred by convolving image with a 5×5 Gaussian filter

Fig. 7 Comparison of proposed method with blind deconvolution methods for artificially blurred MRI corrupted by Poisson noise. Test image was blurred by convolving image with a 5×5 Gaussian filter

Blurred (5x5) and noisy (poisson) image	Proposed method (α=0.05)	SeDDARa (α=0.05 filter 2x2)

13,65±0,04	13,50±0,06	14,34±0,047

Blind RL (PSF 5x5)	Blind RL (PSF mxn)	MAP (PSF 5x5)

15,53±1,43	21,35±0,06	17,22±0,07

Standard deviation of the entropy image σ_{ent} can be defined as a quality metric.

Also, in order to validate our proposed metric, we used Renyi Entropy-based Anisotropic Quality Index (AQI) as a reference quality metric [39]. AQI can evaluate image quality when the images are degraded by both blur and noise. For a sharp image, AQI and σ_{ent} should be as high as possible.
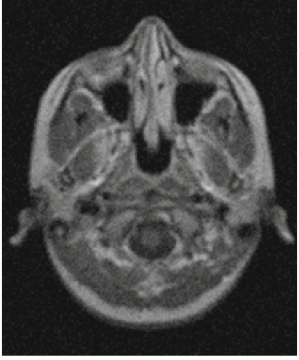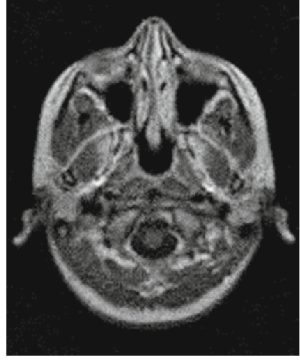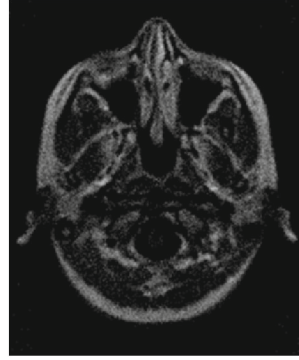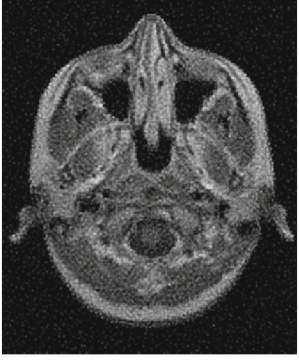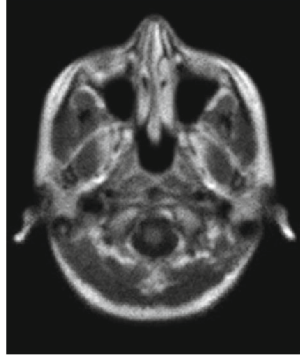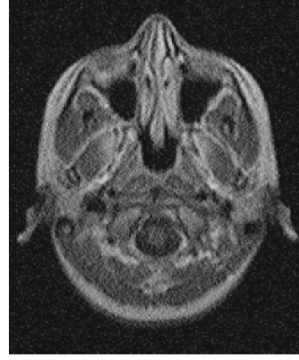
2.7 Experiments

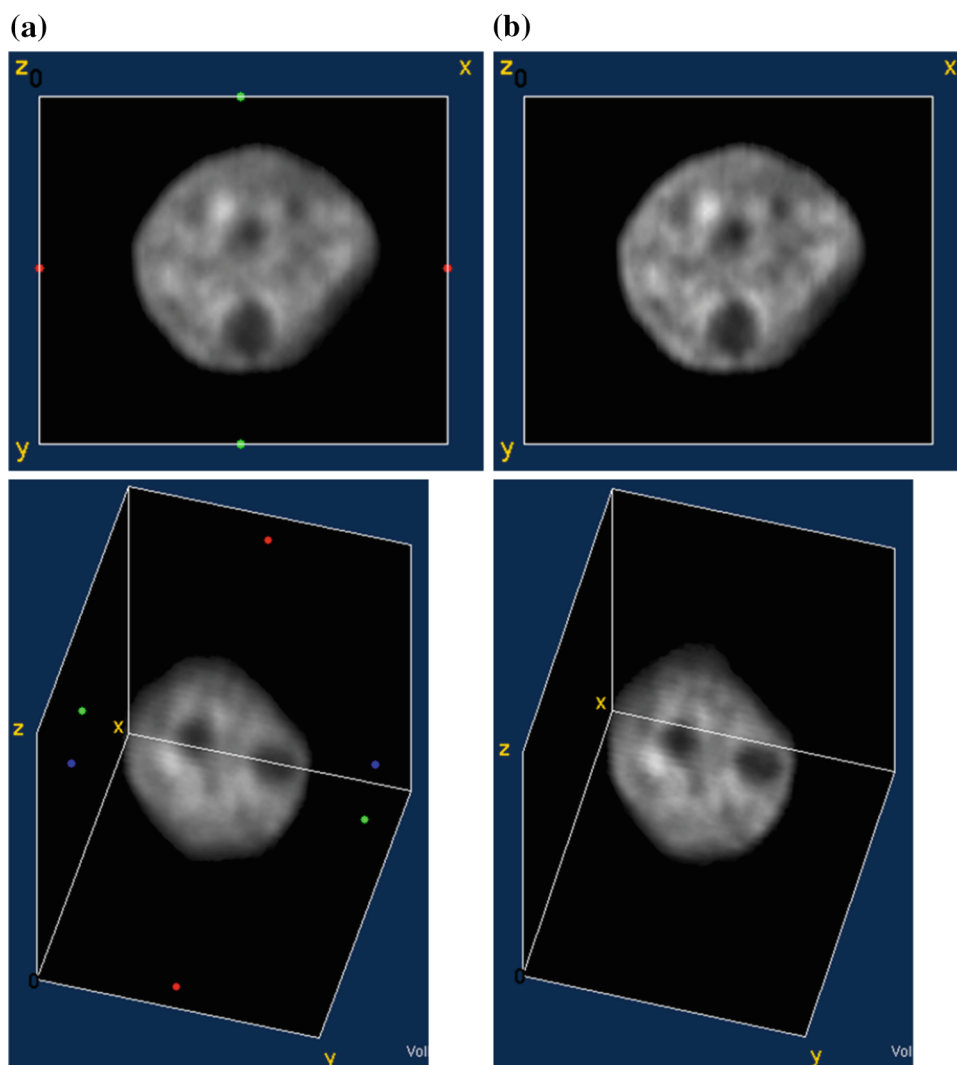A flow diagram illustrating our steps is shown in Fig. 2.

Because our modified deconvolution method includes denoising, we first need to choose the optimum wavelet type for our wavelet-based denoising algorithm. Each of the algorithms was run 100 times; the mean and the standard deviation of the results were recorded. To choose the optimum wavelet type for our proposed denoising approach, test image 1 was degraded with Poisson noise (Tables 1, 2). To compare our proposed denoising approach with several standard denoising approaches, images 1,2,3,4 and 9 were degraded with Poisson noise (Table 3).

Then, we compared our deconvolution method with several deconvolution methods by applying them on artificially blurred and noisy test images. Test image 9 and 1 were

Fig. 8 Comparison of proposed method with blind deconvolution methods for artificially blurred MRI corrupted by Gaussian noise. Test image was blurred by convolving image with a 3 × 3 Gaussian filter

Blurred (3x3) and noisy (gaussian variance: 0.001) image	Proposed method (α=0.1)	SeDDARa (α=0.1 filter 3x3)
10,044±0,032	14,24±0,062	32,77+0.031
Blind RL (PSF 3x3)	Blind RL (PSF mxn)	MAP (PSF 5x5)
17,68±4,14	19,31±0,098	15,65±0,065

Fig. 9 a, **b** 3D reconstructed cell (nucleus) image for different orientations

(a)

(b)

Table 4 Comparison of computational times of the blind methods for an image size of 226 × 186 pixels

Compared methods	SeDDaRa	RL (for 10–100 iterations)	MAP (for 11 iterations)	Proposed method
Computational time (s)	0.71	0.82–6.04	12.5	1.22

blurred by convolving images with a 5 × 5 Gaussian filter and degraded with Poisson noise (Figs. 3, 4). Then, the same images were blurred with a 5 × 5 Gaussian filter and degraded with Gaussian noise (noise variance = 0.001) (Figs. 5, 6). To compare proposed deconvolution method with blind deconvolution methods, image 9 was blurred with 5 × 5 Gaussian filter and degraded with Poisson noise. Then, the same image was blurred with a 3 × 3 Gaussian filter and degraded with Gaussian noise (noise variance = 0.001) (Figs. 7, 8).

Finally, to test our proposed quality metric images 1 to 8 were blurred with 3 × 3, 5 × 5 and 9 × 9 Gaussian filters (Table 5). Then, the same images were blurred and degraded with Gaussian noise (Table 6).

After validating our methods, we applied our proposed methods to cell images obtained with confocal and two photon microscopy (Table 7). Using deblurred and denoised 2D image frames, we reconstructed a three dimensionally illustration of the data (nucleus) with ImageJ Volume Viewer [42] (Fig. 9).

3 Results

3.1 Used denoising method

Our denoising approach is based on the e-median filtering [33,34] in the wavelet domain by using the thresh-

Table 5 Blurring ratio versus quality metrics for noise-free images

Test images	PSF dimension	AQI	σ_{ent}
Image 1	Ref.	1	1
	3	0.5	0.94
	5	0.42	0.92
	9	0.36	0.88
Image 2	Ref.	1	1
	3	0.23	0.87
	5	0.02	0.74
	9	0.01	0.54
Image 3	Ref.	1	1
	3	0.2	0.62
	5	0.05	0.41
	9	0.01	0.22
Image 4	Ref.	1	1
	3	0.22	0.70
	5	0.06	0.51
	9	0.01	0.29
Image 5	Ref.	1	1
	3	0.23	0.92
	5	0.14	0.80
	9	0.08	0.51
Image 6	Ref.	1	1
	3	0.34	0.87
	5	0.13	0.76
	9	0.04	0.57
Image 7	Ref.	1	1
	3	0.35	0.89
	5	0.14	0.70
	9	0.04	0.60
Image 8	Ref.	1	1
	3	0.18	0.61
	5	0.06	0.45
	9	0.01	0.27

Table 6 Blurring ratio versus quality metrics for noisy images

Test images	PSF Dimension	AQI	σ_{ent}
Image 1	3	1	1
	5	0.5	0.74
	9	0.37	0.73
Image 2	3	1	1
	5	0.51	0.90
	9	0.51	0.71
Image 3	3	1	1
	5	0.19	0.67
	9	0.03	0.37
Image 4	3	1	1
	5	0.55	0.74
	9	0.42	0.45
Image 5	3	1	1
	5	0.92	0.87
	9	0.49	0.56
Image 6	3	1	1
	5	0.73	0.88
	9	0.02	0.67
Image 7	3	1	1
	5	0.17	0.94
	9	0.04	0.85
Image 8	3	1	1
	5	0.34	0.76
	9	0.02	0.48

where σ represents the noise variance and N represents the size of the image. Our denoising method and Pure-let use square root of the approximation coefficients at the same scale for the threshold value of wavelet coefficients.

Our method and Pure-let successfully denoised all test images which can be explained by the better threshold selection approaches of these methods.

old values obtained from the approximation coefficients [26,35].

We first evaluated our e-median/wavelet-based denoising method on Poisson and Gaussian corrupted test images. We used different mother wavelet types in our denoising method and compared them in terms RMSE both for DWT and WPT (Tables 1, 2). These comparisons were performed on test image 1 which is degraded with Poisson noise. Minimum error was obtained with coif5 wavelet type. WPT-based algorithm resulted in less error than the DWT-based algorithm.

Also, we compared our method with Donoho's soft and hard thresholding methods and the Pure-let method (Table 3). Standard soft and hard thresholding methods use the global threshold value:

$$T = \sigma\sqrt{2\log(N)} \qquad (15)$$

3.2 Proposed deconvolution method

Our proposed deconvolution method was compared with non-blind (inverse filter, wiener filter, RL-based algorithm) and blind (SeDDaRa, RL-based blind algorithm, MAP based algorithm) deconvolution methods. Comparisons with non-blind methods were performed with blurred and noisy test images in terms of RMSE (Figs. 3, 4 for Poisson and Figs. 5, 6 for Gaussian noise). Also, same comparisons were made with our proposed method and blind deconvolution methods in terms of RMSE and computational time (Figs. 7, 8). Since the inverse filter is a form of a high-pass filter, inverse filtering amplifies the noise that is present in the image. Our method gives the least RMSE for all comparisons.

Table 7 Image enhancement results for cell images obtained with confocal and two photon microscopy

Image type	Wavelet transform type	Image quality metric	Recorded cell images	Deblurred image with proposed method
Confocal fluorescence	DWT	AQI	0.0044	0.0197
		σ_{ent}	0.1528	0.2097
	WPT	AQI	0.0044	0.0172
		σ_{ent}	0.1528	0.2117
Two photon fluorescence	DWT	AQI	0.0029	0.0103
		σ_{ent}	0.0866	0.123
	WPT	AQI	0.0029	0.0140
		σ_{ent}	0.0866	0.123

The computational times of the methods for an image size of 226×186 pixels are given in Table 4. The experiments are performed on a laptop computer configured by Core 2 Duo T6600 2.2 GHz CPU with a 4 GB memory. Since our method is wavelet based, it requires additional computational time compared to the Fourier-based SeDDaRa. But it requires less time than iterative methods (RL and MAP).

We varied α values to evaluate the relation between α and contrast ($\alpha = 0.05$ for Figs. 3, 4 and $\alpha = 0.1$ for Figs. 5, 6). As α increases, contrast increases at the expense of increasing RMSE.

3.3 Proposed image quality metrics

In order to test our proposed image quality metric, we compared σ_{ent} with AQI by increasing blurring ratio both for noiseless and noisy images (Tables 5, 6). As blurring increases, AQI and σ_{ent} decrease. A correlation greater than 0.8 is generally described as strong, whereas a correlation less than 0.5 is generally described as weak. We observed strong correlations between blurring ratio and σ_{ent} as well as σ_{ent} and AQI ($|r| > 0.83$ and $r > 0.8$, indicating that our proposed metric can be used as image quality metric in terms of deblurring.

3.4 Enhancement of cell images

Finally, we applied our deconvolution algorithm on cell images. Evaluation of our method was performed with σ_{ent}. As can be seen from Table 7, our deconvolution method allows to obtain improved image quality in terms of our proposed metric σ_{ent} and AQI. The results with our WPT-based method and DWT method are similar.

After deconvolution of the 2D images of our cells (40 frames), we reconstructed a three-dimensional dataset by using volume rendering with ImageJ Volume Viewer. In order to show enhancement visually, a slice from the stack is given in Fig. 9a, b which shows the recorded and restored image, respectively.

4 Conclusions

Our proposed wavelet transform-based deconvolution method resulted in the least error compared to other methods. The error is minimal because our method includes a denoising process. But our method needs further improvement for better contrast enhancement without amplifying the noise. This could done by modifying our denoising process in an iterative manner.

We were successful in developing a new image quality metric σ_{ent} because there is a good correlation between our entropy-based metric and the blurring ratio. The limitation of our metric is its inability of noise evaluation. It is necessary to evaluate image degradation for both blurring and noise effects. We need to develop a better quality metric which can evaluate both blurring and noise effects together.

Our results show that proposed deconvolution method is applicable to fluorescence microscopy images.

References

1. Wu, Q., Merchant, F.A., Castleman, K.R.: Microscope Image Processing. Academic Press, Amsterdam (2008)
2. Delpretti, S., Luisier, F., Ramani, S., Blu, T., Unser, M.: Multiframe sure-let denoising of timelapse fluorescence microscopy images. In: Biomedical Imaging: From Nano to Macro, 2008. ISBI 2008. 5th IEEE International Symposium on, 14–17 May 2008, pp. 149–152
3. Sarder, P., Nehorai, A.: Deconvolution methods for 3-D fluorescence microscopy images. IEEE Signal Process. Mag. **23**(3), 32–45 (2006)
4. Shah, S.: Deconvolution Algorithms for Fluorescence and Electron Microscopy. University of Michigan, Ann Arbor (2006)
5. Fish, D.A., Brinicombe, A.M., Pike, E.R., Walker, J.G.: Blind deconvolution by means of the Richardson–Lucy algorithm. J. Opt. Soc. Am. A Opt. Image Sci. Vis. **12**(1), 58–65 (1995). doi:10.1364/josaa.12.000058
6. Lanteri, H., Aime, C., Beaumont, H., Gaucherel, P.: Blind deconvolution using the Richardson-Lucy algorithm, vol. 2312. Optics in Atmospheric Propagation and Random Phenomena. SPIE—Int Soc Optical Engineering, Bellingham (1994)

7. Fan, F., Yang, K., Xia, M., Li, W., Fu, B., Zhang, W.: Comparative study on several blind deconvolution algorithms applied to underwater image restoration. Opt. Rev. **17**(3), 123–129 (2010). doi:10.1007/s10043-010-0022-7

8. Levin, A., Weiss, Y., Durand, F., Freeman, W.T.: Efficient marginal likelihood optimization in blind deconvolution. In: Computer Vision and Pattern Recognition (CVPR), 2011 IEEE Conference on, 20–25 June 2011, pp. 2657–2664

9. Fergus, R., Singh, B., Hertzmann, A., Roweis, S.T., Freeman, W.T.: Removing camera shake from a single photograph. ACM Trans. Graph. **25**(3), 787–794 (2006)

10. Caron, J.N., Namazi, N.M., Rollins, C.J.: Noniterative blind data restoration by use of an extracted filter function. Appl. Opt. **41**(32), 6884–6889 (2002)

11. Caron, J.N.: Application of SeDDaRA Blind Deconvolution for Efficient Improvement of Confocal Microscopy Images. Quarktet Technical Note (2011)

12. Boutet de Monvel, J., Le Calvez, S., Ulfendahl, M.: Image restoration for confocal microscopy: improving the limits of deconvolution, with application to the visualization of the mammalian hearing organ. Biophys. J. **80**(5), 2455–2470 (2001). doi:10.1016/S0006-3495(01)76214-5

13. Nowak, R.D., Baraniuk, R.G.: Wavelet-domain filtering for photon imaging systems. IEEE Trans. Image Process. **8**(5), 666–678 (1999). doi:10.1109/83.760334

14. Starck, J.-L., Bijaoui, A.: Filtering and deconvolution by the wavelet transform. Signal Process. **35**(3), 195–211 (1994)

15. Bernas, T., Asem, E.K., Robinson, J.P., Rajwa, B.: Compression of fluorescence microscopy images based on the signal-to-noise estimation. Microsc. Res. Tech. **69**(1), 1–9 (2006). doi:10.1002/jemt.20259

16. Grgic, S., Grgic, M., Zovko-Cihlar, B.: Performance analysis of image compression using wavelets. IEEE Trans. Ind. Electron. **48**(3), 682–695 (2001)

17. Shapiro, J.M.: Embedded image coding using zerotrees of wavelet coefficients. IEEE Trans. Signal Process. **41**(12), 3445–3462 (1993)

18. Willett, R.M., Nowak, R.D.: Platelets: a multiscale approach for recovering edges and surfaces in photon-limited medical imaging. IEEE Trans. Med. Imaging **22**(3), 332–350 (2003)

19. Colicchio, B., Maalouf, E., Haeberle, O., Dieterlen, A.: Wavelet filtering applied to 3D wide field fluorescence microscopy deconvolution. In: PSIP'07, Mulhouse, France 2007

20. Chaux, C., Blanc-Féraud, L., Zerubia, J.: Wavelet-based restoration methods: application to 3D confocal microscopy images. In: Van De Ville, D., Goyal, V. K., Papadakis, M. (eds.) SPIE 2007 Wavelets XII, vol. 6701, p. 67010E. SPIE, San Diego, CA, USA (2007). doi:10.1117/12.731438

21. Larson, J.M.: 2D and 3D deconvolution of confocal fluorescence images by maximum likelihood estimation. 86–94 (2002). doi:10.1117/12.467835

22. Biggs, D.S.C.: Clearing up deconvolution. In: Biophotonics International, vol. 11. vol. 2, p. 32(36) (2004)

23. Laksameethanasan, D., Brandt, S.S., Renaud, O., Shorte, S.L.: Dual filtered backprojection for micro-rotation confocal microscopy. Inverse Probl. **25**(1), 1–17 (2009). doi:10.1088/0266-5611/25/1/015006

24. Wallace, W., Schaefer, L.H., Swedlow, J.R.: A workingperson's guide to deconvolution in light microscopy. Biotechniques **31**(5), 1076 (2001)

25. Donoho, D.L., Johnstone, I.M.: Threshold selection for wavelet shrinkage of noisy data. In: Engineering in Medicine and Biology Society, 1994. Engineering Advances: New Opportunities for Biomedical Engineers. Proceedings of the 16th Annual International Conference of the IEEE, 3–6 Nov 1994 1994, vol. 21, pp. A24–A25

26. Luisier, F., Vonesch, C., Blu, T., Unser, M.: Fast interscale wavelet denoising of Poisson-corrupted images. Signal Process. **90**(2), 415–427 (2010). doi:10.1016/j.sigpro.2009.07.009

27. Jain, A.K.: Fundamentals of Digital Image Processing. Prentice-Hall, New York (1989)

28. Lim, J.S.: Two-Dimensional Signal and Image Processing. Prentice-Hall, New York (1990)

29. Luo, G.: Fast wavelet image denoising based on local variance and edge analysis. Int. J. Intell. Technol. **1**(2), 165–175 (2006)

30. Silva, R., Minetto, R., Schwartz, W., Pedrini, H.: Adaptive edge-preserving image denoising using wavelet transforms. Pattern Anal. Appl. 1–14 (2012). doi:10.1007/s10044-012-0266-x

31. Gonzalez, R.C., Woods, R.E.: Digital Image Processing. Pearson/Prentice Hall, New York (2008)

32. Mallat, S.G., Peyré, G.: A Wavelet Tour of Signal Processing: The Sparse Way, 2nd edn. Academic Press, Burlington, MA, USA (2009)

33. Haseyama, M., Takezawa, M., Kondo, K., Kitajima, H.: Ieee: An image restoration method using IFS. In: 2000 International Conference on Image Processing, Vol Iii, Proceedings (2000)

34. Koç, S., Ergelebi, E.: Image restoration by lifting-based wavelet domain E-median filter, vol. 28. Taejon, COREE, REPUBLIQUE DE, Electronics and Telecommunications Research Institute (2006)

35. Fryzlewicz, P., Nason, G.P.: A Haar-Fisz algorithm for Poisson intensity estimation. J. Comput. Graph. Stat. **13**(3), 621–638 (2004). doi:10.1198/106186004X2697

36. Donoho, D.: De-noising by soft-thresholding. IEEE Trans. Inform. Theory **41**, 613–627 (1995)

37. Donoho, D.L.: Wavelet shrinkage and W.V.D.: a 10-minute tour. Paper presented at the Progress in Wavelet Analysis and Applications

38. Coifman, R.R., Donoho, D.L.: Translation-invariant de-noising. Paper presented at the in Wavelets and Statistics, Lecture Notes in Statistics 103

39. Gabarda, S., Cristobal, G.: Blind image quality assessment through anisotropy. J. Opt. Soc. Am. A Opt. Image Sci. Vis. **24**(12), B42–51 (2007)

40. De, I., Sil, J.: Wavelet entropy based no-reference quality prediction of distorted/decompressed images. In: Computer Engineering and Technology (ICCET), 2010 2nd International Conference on, 16–18 April 2010 2010, pp. V3–245–V243-250

41. Yordanova, J., Kolev, V., Rosso, O.A., Schurmann, M., Sakowitz, O.W., Ozgoren, M., Basar, E.: Wavelet entropy analysis of event-related potentials indicates modality-independent theta dominance. J. Neurosci. Meth. **117**(1), 99–109 (2002). doi:10.1016/S0165-0270(02)00095-X

42. Barthel, K.U.: Volume Viewer. http://rsb.info.nih.gov/ij/plugins/volume-viewer.html (2005)